VIII International Conference on Textile Composites and Inflatable Structures
STRUCTURAL MEMBRANES 2017
K.-U.Bletzinger, E. Oñate and B. Kröplin (Eds)

ADVANCED APPROACHES FOR ANALYSIS AND FORM FINDING OF MEMBRANE STRUCTURES WITH FINITE ELEMENTS

Jan Gade[+], Manfred Bischoff[+] and Roman Kemmler[*]

[+] Institute for Structural Mechanics
University of Stuttgart
Pfaffenwaldring 7, 70550 Stuttgart, Germany
e-mails: Bischoff/Gade@ibb.uni-stuttgart.de - web page: https://www.ibb.uni-stuttgart.de/

[*] Professorship for Engineering Mechanics and Structural Analysis
Hochschule Konstanz University of Applied Sciences
Alfred-Wachtel-Straße 8, 78462 Konstanz, Germany
e-mail: Roman.Kemmler@htwg-konstanz.de - web page: http://www.htwg-konstanz.de/

Key words: Woven fabric membranes, microstructural modelling, anisotropic hyperelasticity, parameter identification, form finding, cutting patterning, optimisation

Abstract. *Part I* deals with material modelling of woven fabric membranes. Due to their structure of crossed yarns embedded in coating, woven fabric membranes are characterised by a highly nonlinear stress-strain behaviour. In order to determine an accurate structural response of membrane structures, a suitable description of the material behaviour is required. A linear elastic orthotropic model approach, which is current practice, only allows a relative coarse approximation of the material behaviour. The present work focuses on two different material approaches: A first approach becomes evident by focusing on the meso-scale. The inhomogeneous, however periodic structure of woven fabrics motivates for microstructural modelling. An established microstructural model is considered and enhanced with regard to the coating stiffness. Secondly, an anisotropic hyperelastic material model for woven fabric membranes is considered. By performing inverse processes of parameter identification, fits of the two different material models w.r.t. measured data from a common biaxial test are shown. The results of the inversely parametrised material models are compared and discussed.

Part II presents an extended approach for a simultaneous form finding and cutting patterning computation of membrane structures. The approach is formulated as an optimisation problem in which both the geometries of the equilibrium and cutting patterning configuration are initially unknown. The design objectives are minimum deviations from prescribed stresses in warp and fill direction along with minimum shear deformation. The equilibrium equations are introduced into the optimisation problem as constraints. Additional design criteria can be formulated (for the geometry of seam lines etc.). Similar to

the motivation for the Updated Reference Strategy [4] the described problem is singular in the tangent plane. In both the equilibrium and the cutting patterning configuration finite element nodes can move without changing stresses. Therefore, several approaches are presented to stabilise the algorithm. The overall result of the computation is a stressed equilibrium and an unstressed cutting patterning geometry. The interaction of both configurations is described in Total Lagrangian formulation.

The microstructural model, which is focused in Part I, is applied. Based on this approach, information about fibre orientation as well as the ending of fibres at cutting edges are available. As a result, more accurate results can be computed compared to simpler approaches commonly used in practice.

Part I: Comparison of a microstructural model with an anisotropic hyperelastic model gained by inverse problems of parameter identification

1 INTRODUCTION

The structure of a woven fabric embedded in coating, which is caused by the manufacturing process, leads to a significant physically nonlinear material behaviour. Moreover, membrane structures are characterised by a pronounced geometrically nonlinear behavior as well. Hence, a realistic analysis demands for a suitable modelling of the material behaviour in context of finite deformations theory. For this purpose there are several approaches, which arise from different modelling scales.

At first, the test data from a biaxial tension test is presented with regard to its usage in parameter identification (Chapter 2). In Chapter 3 we give just the basic ideas about approaches for modelling material behaviour on different modelling scales. After that, we firstly present an established microstructural model with our enhancement (Chapter 4) and we secondly pose an anisotropic hyperelastic model (Chapter 5). In Chapter 6 the processes of identification of the model parameters are outlined. Finally, the results of the two material models are compared and discussed (Chapter 7). The contribution focuses on the elastic deformation behaviour. Neither viscoelastic, viscoplastic nor wrinkling effects are considered.

2 EXPERIMENTAL DATA FROM A BIAXIAL TENSION TEST

In order to perform the identification of the parameters of the microstructural model (Chapter 6) as well as the anisotropic hyperelastic model (Chapter 5), data from a biaxial tension test are considered. The test data was kindly provided by Low and Bonar GmbH (former Mehler Texnologies GmbH, Fulda/Germany). Figure 1 outlines the setup of the test. The specimen is a slotted woven fabric membrane, whose two families of fibres are orthogonal and orientated parallel to the load directions.

The test procedure as well as the evaluation method is performed in accordance to JIS

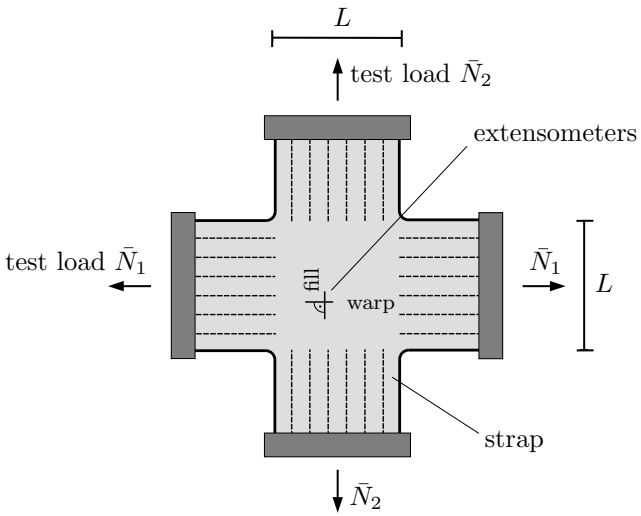

Figure 1: Biaxial tension test of a woven fabric membrane – outline of the setup (after [1])

MSAJ/M-02-1995 [14]. This means that load-strain curves corresponding to 5 load ratios are extracted for further regards. These 5 load ratios $(\bar{N}_{1,i}/L) : (\bar{N}_{2,i}/L)$ are 2:1, 1:2, 2:0, 2:2 and 0:2, where the ratio value of 2 resp. 1 is equivalent to a load of 45.0 resp. 22.5 kN/m. It is a load-controlled test with a constant loading rate of +/–0.2 kN/(m s), which is assumed to be a quasi-static loading process. Since the loads are related to a reference dimension L, they act as first Piola-Kirchhoff stresses. Therefore, $\bar{P}_{11,i} := \bar{N}_{1,i}/L$ resp. $\bar{P}_{22,i} := \bar{N}_{2,i}/L$ (with regard to unit thickness) is assumed. Engineering strains are measured with extensometers in the inner area of the specimen. They are aligned parallel to the directions of the yarns. More details concerning the biaxial tension test, the specific test procedure and evaluation method are given in e.g. [7, pp. 51f.], [16, pp. 382f.].

There are a total of $n_V = 380$ test data points indexed by the symbol $i = 1, \ldots, n_V$. The measured and evaluated test data is shown in Figure 5. $\bar{\lambda}_{11,i}$ resp. $\bar{\lambda}_{22,i}$ is the i-th measured stretching in warp resp. fill direction (note: stretch λ = engineering strain + 1).

3 MODELLING APPROACHES FOR WOVEN FABRIC MATERIALS

Considering woven fabric materials in an engineering context, three distinct approaches can be utilised to model the stress-strain behavior accounting for the material structure:

(a) Micro-scale approach The modelling of the particular components of the material (yarns, coating, contact) is applicable for determination of local phenomena like e.g. failure or damage behaviour.

(b) Macro-scale approach The assumption of a phenomenological material model like a linear elastic, orthotropic model is a basic engineering approach and is used in practical applications. A hyperelastic material model falls in this category as well. The material parameters have to be determined by means of experimental methods

(e.g. [18], [7], [16]).

(c) Meso-scale approach Since a woven fabric membrane is characterised by a repetitive structure, the modelling of the material behaviour by means of a submodel at the meso-scale is reasonable. Such a submodel represents the smallest repetitive unit and is called a unit cell model or microstructural model (e.g. [5], [6], [1]).

In the present contribution, approach (c) is focused by assuming a microstructural model for plain-woven fabric materials. Inversely gained results are compared with results of an anisotropic hyperelastic material model (approach (b)). In order to perform numerical computations of full scale engineering structures, the microstructural model at the meso-scale (approach (c)) is coupled with the macro-scale in context of e.g. finite element computations (see Part II, Figure 6). Such an approach is denoted as multi-scale modelling or FE^2 ([9]).

4 MICROSTRUCTURAL MODEL

In this section an established microstructural model is stated, enhanced and at last the governing model equations are mentioned.

4.1 Established model

The basis of Part I of the present contribution is the established microstructural model for plain-woven fabric membrane materials shown in Figure 2. An early publication of a

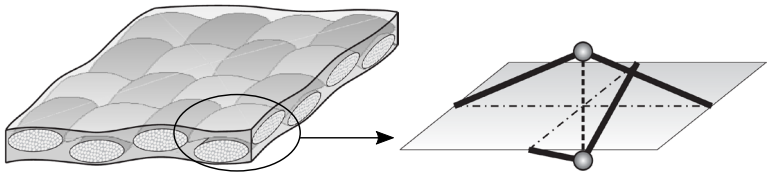

Figure 2: Left: Plain-woven fabric membrane; right: established microstructural model (from [1, p. 17])

mechanical description of the model is attributed to Kawabata [12]. He modelled one single intersection point as inclined, piecewise linear bar elements coupled by another bar element, which represents the contact between the yarns. Amongst others, there were Meffert [13] as well as Blum [5], who made further studies of the above-mentioned model. On this basis, Bögner reveals a considerable influence of the transversal compression of the yarns. Therefore she modelled a spring in between the two intersection points of the yarns [6]. Recently, Kaiser/Haug/Pyttel/Duddeck [11] used a beam model with bending stiffness as representatives for the yarns. They couple it with a finite element system and handle draping simulation problems by using material properties from earlier publications.

A methodological feature of the work mentioned above is, that the geometrical as well as the stiffness parameters of the models are directly obtained by means of experimental

methods. This means that for example geometrical dimensions of the particular woven fabric like yarn diameters and yarn spacings were obtained by means of experimental measurement. In contrast to this, in the present paper model parameters are gained as solutions of inverse problems on the basis of test data of a standardised biaxial tension test (see Chapter 6). An advantage is the flexible adaption to other test data. Moreover, there is no need for special measurement equipment. On the other hand, a direct physical meaning of the determined parameters is not ensured at all times.

4.2 Enhancement of the established model

A well-described deformation mechanism is the crimp interchange (e.g. [7], [1]), which is essentially responsible for the nonlinear material behaviour. Figure 3 outlines the mechanism in context of the established unit cell modell. In cases, where the load in one direction dominates (e.g. $F_1 \ll F_2$), the coating is lengthened resp. shortened and tension resp. compression stresses are activated, whose magnitudes are functions of the coating stiffness and contact stiffness of the yarns. Hence, the model is enhanced by

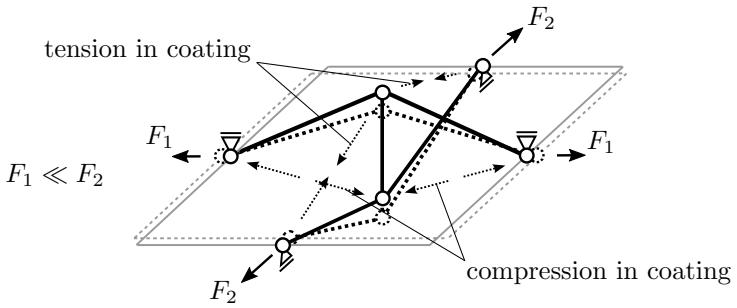

Figure 3: Deformation of the established model during crimp interchange

springs representing the stiffness in as well as perpendicular to the model plane. The entire model is illustrated in Figure 4. It is explained in the subsequent section. During the parameter identification process (see Chapter 6) the spring elements turned out to be the decisive elements in order to obtain results with a high accuracy in comparison with the test data.

4.3 Structural analysis of the enhanced model

The enhanced model is shown in Figure 4. The blue resp. red bar elements represent the yarns, the green bar models the contact and the spring elements make consideration of the stiffness of the coating. Moreover, the geometric dimensions of the model are parametrised. The following eleven model parameters are assumed, at which the dimension L_1 serves as a reference quantity of the model:

- Relative dimensions L_2, H_1 und H_2 (physical unit: $[L_1]$);
- relative extensional stiffnesses $k_{y,1}$, $k_{y,2}$ and k_c (physical unit: [force]);

- relative spring stiffnesses $c_{A,1}$, $c_{A,2}$, $c_{N,12}$ and $c_{N,21}$ (physical unit: [force]/[L_1]).

All parameters are posed in $\boldsymbol{M}_{mic} := \left[L_1 \;\; L_2 \;\; H_1 \;\; H_2 \;\; k_{y,1} \;\; k_{y,2} \;\; k_c \;\; c_{A,1} \;\; c_{A,2} \;\; c_{N,12} \;\; c_{N,21} \right]^T$. The index '1' corresponds to the warp direction whereas the index '2' refers to the fill direction. It is assumed, that the microstructure represents the smallest unit of the material, whose force-strain behaviour does not depend on the characteristic dimension, here L_1. Hence, there is no need to define a certain physical unit for L_1. The deformation behaviour is symmetric and is therefore determined by four displacements, $\boldsymbol{u} = \left[u_1 \;\; u_2 \;\; u_3 \;\; u_4 \right]^T$.

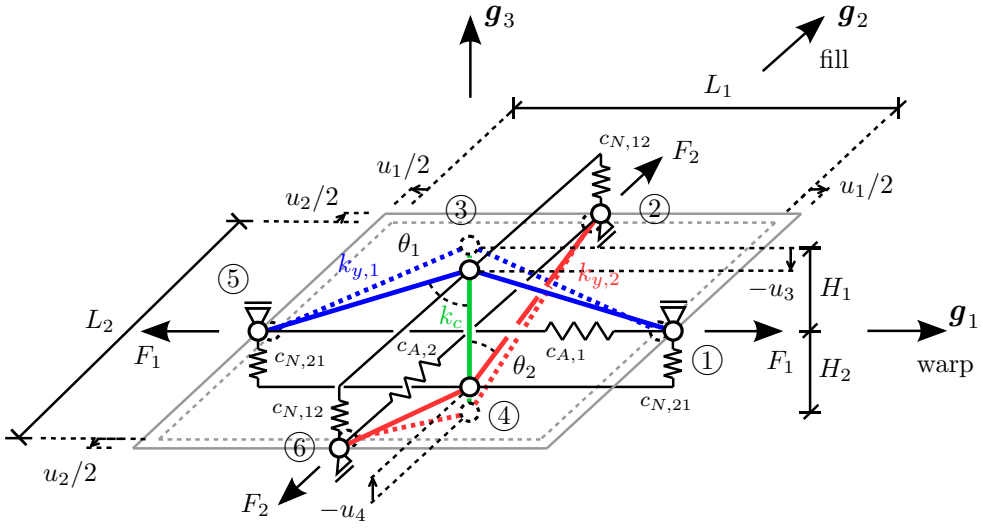

Figure 4: Microstructural model – undeformed and deformed configuration

Kinematic equations Nonlinear kinematics is applied to relate the displacements $\boldsymbol{u}$ with the strains resp. elongations of the bar resp. spring elements. These equations are partially nonlinear in L_1, L_2, H_1, H_2 and $\boldsymbol{u}$.

Constitutive equations Linear equations, which plug element forces and strains resp. elongations, are assumed. Hence, the constitutive equations are linear in $k_{y,1}$, $k_{y,2}$, k_c, $c_{A,1}$, $c_{A,2}$, $c_{N,12}$ und $c_{N,21}$.

Equilibrium Equilibrium of forces at joints ①, ②, ③ und ④ yield four independent nonlinear equations in $\boldsymbol{u}$:

$$\boldsymbol{G}\left(\boldsymbol{u}\right) = \boldsymbol{F}_{\text{int}}\left(\boldsymbol{u}\right) - \boldsymbol{F}_{\text{ext}} \stackrel{!}{=} \boldsymbol{0} \; . \tag{1}$$

The residual force vector $\boldsymbol{G}$ is a vector-valued, continuously differentiable nonlinear function in $\boldsymbol{u}$. $\boldsymbol{F}_{\text{int}}$ means the vector of internal forces and $\boldsymbol{F}_{\text{ext}}$ denotes the vector of external forces. With regard to the parameter identification the nodal forces are assumed to be $F_1 = \bar{P}_{11,i}\, L_2$ resp. $F_2 = \bar{P}_{22,i}\, L_1$.

Solution One may solve the nonlinear system of equations (Eq. (1)) for each set of test data $i = 1, \ldots, n_V$ by using a Newton-Raphson iteration scheme (equilibrium iteration), wherein the tangential stiffness matrix $\mathbf{K}_\mathrm{T} = \partial \boldsymbol{G} / \partial \boldsymbol{u}$ occurs. The corresponding stretching $\boldsymbol{\lambda}_i$ is computed as

$$\boldsymbol{\lambda}_i = [\, \lambda_{11,i} \;\; \lambda_{22,i} \,]^T \,, \quad \lambda_{dd,i} = \lambda_{dd,i}\,(\boldsymbol{u}) = \frac{u_{d,i}}{L_d} + 1 \,, \quad d = 1, 2 \,. \tag{2}$$

5 ANISOTROPIC HYPERELASTIC MODEL

In an alternative approach, a woven fabric membrane material is presumed to behave anisotropic hyperelastic. Holzapfel assumes a form of an energy function for an anisotropically hyperelastic material with two families of fibres to be

$$\psi = \psi(\mathbf{C}, \mathbf{M}_{(1)}, \mathbf{M}_{(2)}) = \psi(\mathbf{Q}^T \mathbf{C} \mathbf{Q}, \mathbf{Q}^T \mathbf{M}_{(1)} \mathbf{Q}, \mathbf{Q}^T \mathbf{M}_{(2)} \mathbf{Q}) \,. \tag{3}$$

ψ is an isotropic tensor function in $(\mathbf{C}, \mathbf{M}_{(1)}, \mathbf{M}_{(2)})$, if Eq. (3) holds for all proper orthogonal transformation tensors $\mathbf{Q}$ [10, pp. 273ff.]. $\mathbf{C}$ is the right Cauchy-Green deformation tensor. Hence, the energy is invariant w.r.t. $\mathbf{C}, \mathbf{M}_{(1)}$ and $\mathbf{M}_{(2)}$, wherein the so-called structural tensors $\mathbf{M}_{(d)} = \boldsymbol{a}_{(d)} \otimes \boldsymbol{a}_{(d)}$ $(d = 1, 2)$ specify the symmetries of the material. The directions of fibres are represented by $\boldsymbol{a}_{(d)}$. Such an energy can in general be formulated in terms of nine invariants. In most woven fabric materials the two families of fibres (warp resp. fill) can be assumed to be orthogonal, $\boldsymbol{a}_{(1)} \cdot \boldsymbol{a}_{(2)} = 0$. The orthogonality yields ψ to be a function of only the first seven invariants:

$$\psi = \psi(\mathbf{C}, \mathbf{M}_{(1)}, \mathbf{M}_{(2)}) = \psi(I_1, I_2, I_3, J_4^{(1)}, J_5^{(1)}, J_4^{(2)}, J_5^{(2)}) \,, \quad d = 1, 2 \tag{4}$$

$$I_1 := \mathrm{tr}(\mathbf{C}) \,, \; I_2 := \mathrm{tr}(\mathrm{Cof}\mathbf{C}) \,, \; I_3 := \det(\mathbf{C}) \,, \; J_4^{(d)} := \mathrm{tr}(\mathbf{C}\mathbf{M}_{(d)}) \,, \; J_5^{(d)} := \mathrm{tr}(\mathbf{C}^2 \mathbf{M}_{(d)})$$

Amongst others, [2] derives an energy function which fulfils Eq. (4):

$$\psi = \psi_\mathrm{iso} + \sum_{d=1,2} \psi_\mathrm{ti}^{(d)} \,, \quad d = 1, 2 \tag{5}$$

$$\psi_\mathrm{iso}\,(I_1, I_3) = c_1 \left(\frac{I_1}{{I_3}^{1/3}} - 3 \right) + \varepsilon_1 \left({I_3}^{\varepsilon_2} + \frac{1}{{I_3}^{\varepsilon_2}} - 2 \right) \,, \quad c_1 > 0 \,, \; \varepsilon_1 > 0 \,, \; \varepsilon_2 > 1 \,,$$

$$\psi_\mathrm{ti}^{(d)} \left(J_4^{(d)} \right) = \begin{cases} \alpha_1^{(d)} \left(J_4^{(d)} - 1 \right)^{\alpha_2^{(d)}} & \text{for } J_4^{(d)} > 1 \\ 0 & \text{for } J_4^{(d)} \leq 1 \end{cases} \,, \quad \alpha_1^{(d)} \geq 0 \,, \; \alpha_2^{(d)} > 1$$

Eq. (4) is an additive decomposition in an isotropic part ψ_iso and two discontiuous, transversal isotropic parts $\psi_\mathrm{ti}^{(d)}$, each of them corresponding to a certain fibre family. The decomposition is motivated by constitution of a woven fabric material, which is made of a relatively weak matrix materials and two orthogonal families of stiff fibres [3,

p. 1021]. In [2] it is proved, that this energy function is convex in all arguments (polyconvexity) and therefore stable. The meaning of each of the seven material parameters $\boldsymbol{M}_{\text{hyp}} := [\, c_1 \;\varepsilon_1 \;\varepsilon_2 \;\alpha_1^{(1)} \;\alpha_2^{(1)} \;\alpha_1^{(2)} \;\alpha_2^{(2)} \,]^T$ and the case distinction in Eq. (5) is explained in [2, pp. 6058, 6064]. Based on the energy function Eq. (5) second resp. first Piola-Kirchhoff stresses $\mathbf{S}$ resp. $\mathbf{P}$ as well as the material tangent tensor $\mathbb{C}$ can be computed from the deformation state, which is assumed to be characterised by right Cauchy-Green deformation tensor $\mathbf{C}$ resp. deformation gradient $\mathbf{F}$ resp. right stretching tensor $\mathbf{U}$ (see [3]):

$$\mathbf{S} = 2\,\frac{\partial \psi(\mathbf{C}, \mathbf{M}_{(1)}, \mathbf{M}_{(2)})}{\partial \mathbf{C}} = \sum_{j,k=1}^{3} S_{jk}\, \boldsymbol{e}_j \otimes \boldsymbol{e}_k\,, \quad \mathbb{C} = 4\,\frac{\partial^2 \psi}{\partial \mathbf{C} \partial \mathbf{C}} \tag{6}$$

$$\mathbf{P} = \mathbf{F}\,\mathbf{S} = \sum_{j,k=1}^{3} P_{jk}\, \boldsymbol{e}_j \otimes \boldsymbol{e}_k\,, \quad \mathbf{C} = \mathbf{F}^T\mathbf{F} = \mathbf{U}^2\,, \quad \mathbf{U} = \sum_{j,k=1}^{3} \lambda_{jk}\, \boldsymbol{e}_j \otimes \boldsymbol{e}_k \tag{7}$$

$\mathbf{S}$ and $\mathbb{C}$ pose the expressions for the corresponding constitutive model for an anisotropic hyperelastic material with two orthogonal families of fibres. This approach has been used in several publications, e.g. [17], [16], [3].

As described so far, the constitutive model is valid for a 3d continuum. Since the assumption of a 2d plane stress state ($P_{j3} = P_{3j} = 0\,,\; j = 1,2,3$) is reasonable for a woven fabric material, the constitutive model has still to be condensed. While neglecting shear deformation ($\lambda_{jk} = \lambda_{kj} = 0\,,\; j,k = 1,2,3\,,\; \beta \neq \gamma$) and consequently obtaining no shear stresses ($\Rightarrow S_{\beta\gamma} = S_{\gamma\beta} = P_{\beta\gamma} = P_{\gamma\beta} = 0\,,\; \beta,\gamma = 1,2\,,\; \beta \neq \gamma$) of the woven fabric material, the remaining three deformation quantities – namely the stretches $\lambda_{11}, \lambda_{22}, \lambda_{33}$ – can be computed from firstly the zero-stress condition in transversal direction and secondly two conditions with regard to the imposed loads in the biaxial tension test $\bar{P}_{11,i} = \bar{N}_{1,i}/L$ resp. $\bar{P}_{22,i} = \bar{N}_{2,i}/L$ (w.r.t. unit thickness). These three conditions are collected in a residuum vector:

$$\boldsymbol{R} = \boldsymbol{R}\,(\boldsymbol{\lambda}_i, \lambda_{33}) := \begin{bmatrix} P_{33} \\ P_{11} - \bar{P}_{11,i} \\ P_{22} - \bar{P}_{22,i} \end{bmatrix} \stackrel{!}{=} \mathbf{0}\,, \quad \boldsymbol{\lambda}_i = [\, \lambda_{11,i} \;\lambda_{22,i} \,]^T \tag{8}$$

The stretches can be computed for each set of test data $i = 1, \ldots, n_{\text{V}}$ by applying a linearisation and performing a subsequent Newton-Raphson iteration scheme. Herein, the Jacobian of $\boldsymbol{R}$ w.r.t. the stretches can be calculated considering the case distinction in Eq. (5).

6 PARAMETER IDENTIFICATION PROCESSES

In order to identify the parameters of the microstructural model, resp. the parameters of the anisotropic hyperelastic model in such a way, that they fit the load-stretch data from the biaxial tension test (see Figure 5), two different inverse problems are formulated analogously. Since the number of test data points is in general greater than the number

of identifiable model parameters, a problem of parameter identification is overdetermined and therefore is treated by methods of optimisation. Subsequently, the optimisation problem is formulated (Section 6.1), the used algorithms are mentioned briefly (Section 6.2) and the resulting model parameters are presented and discussed (Section 6.3).

6.1 Formulation and solution of the inverse problems

The design vector $\boldsymbol{s}_{\mathrm{mic}}$ resp. $\boldsymbol{s}_{\mathrm{hyp}}$ contain the model parameters $\boldsymbol{M}_{\mathrm{mic}}$ resp. $\boldsymbol{M}_{\mathrm{hyp}}$, which shall be identified. The particular objective function f_{mic} resp. f_{hyp} equals the sum of squared errors and yields

$$f_{(\cdot)} = f_{(\cdot)}\left(\boldsymbol{\lambda}_i(\boldsymbol{s}_{(\cdot)}), \ldots, \boldsymbol{\lambda}_{n_{\mathrm{V}}}(\boldsymbol{s}_{(\cdot)})\right) = \sum_{i=1}^{n_{\mathrm{V}}} \left[w_i \underbrace{\left(\lambda_{11,i} - \bar{\lambda}_{11,i}\right)^2}_{\substack{i\text{-th squared error} \\ \text{in warp direction}}} + w_i \underbrace{\left(\lambda_{22,i} - \bar{\lambda}_{22,i}\right)^2}_{\substack{i\text{-th squared error} \\ \text{in fill direction}}} \right]. \quad (9)$$

$\bar{\lambda}_{dd,i}$ is the i-th measured stretch. $\lambda_{dd,i}$ is the corresponding computed stretch (see Eq. (2) resp. Eq. (8)). w_i is the i-th weighting factor ($w_i \in \mathbb{R}^+$). The particular least-squares optimisation problem yields

$$\min_{\boldsymbol{s}_{(\cdot)}} f_{(\cdot)}\left(\boldsymbol{\lambda}_i(\boldsymbol{s}_{(\cdot)}), \ldots, \boldsymbol{\lambda}_{n_{\mathrm{V}}}(\boldsymbol{s}_{(\cdot)})\right). \quad (10)$$

6.2 Substantial aspects towards solution of the inverse problems

The necessary condition for stationarity of the particular problem Eq. (10) is:

$$\nabla_{\boldsymbol{s}_{(\cdot)}} f_{(\cdot)} \stackrel{!}{=} \boldsymbol{0} \;\Leftrightarrow\; \boldsymbol{s}_{(\cdot)} \text{ is a minimum, maximum or saddle point} \quad (11)$$

$\nabla_{\boldsymbol{s}_{(\cdot)}} f_{(\cdot)}$ is the particular gradient of $f_{(\cdot)}$ w.r.t. $\boldsymbol{s}_{(\cdot)}$ and therefore it contains first derivatives $\mathrm{d}\lambda_{dd,i}/\mathrm{d}s_{(\cdot),j}$. For the microstructural model, where $\lambda_{dd,i} = \lambda_{dd,i}\left(\boldsymbol{s}_{\mathrm{mic}}, \boldsymbol{u}(\boldsymbol{s}_{\mathrm{mic}})\right)$, the chain rule yields

$$\frac{\mathrm{d}\lambda_{dd,i}}{\mathrm{d}s_{\mathrm{mic},j}} = \frac{\partial \lambda_{dd,i}}{\partial s_{\mathrm{mic},j}} + \left(\frac{\partial \lambda_{dd,i}}{\partial \boldsymbol{u}}\right)^T \frac{\partial \boldsymbol{u}}{\partial s_{\mathrm{mic},j}}, \quad d = 1, 2.$$

The implicit derivatives $\partial \boldsymbol{u}/\partial s_{\mathrm{mic},j}$ are computed as analytical expressions by performing a direct sensitivity analysis. The explicit derivatives result from Eq. (2) without further explanations. For the hyperelastic model, the required derivatives can be computed analogously.

The particular solution vector $\boldsymbol{s}_{(\cdot)}^*$ is computed based on linearisation of Eq. (11) and subsequent application of an iteration scheme. $\boldsymbol{s}_{(\cdot)}^*$ is a (local) minimum of Eq. (10), if and only if the sufficient condition for a minimum

$$\boldsymbol{s}_{(\cdot)}^{*T} \mathbf{H}_{f_{(\cdot)}, \boldsymbol{s}_{(\cdot)}, k^*} \boldsymbol{s}_{(\cdot)}^* > 0 \quad \Leftrightarrow \quad \mathbf{H}_{f_{(\cdot)}, \boldsymbol{s}_{(\cdot)}, k^*} \text{ positive definite}$$

is fulfilled in addition to Eq. (11). Herein, $\mathbf{H}_{f_{(\cdot)}, \boldsymbol{s}_{(\cdot)}, k^*}$ means the particular Hessian matrix of $f_{(\cdot)}$ w.r.t. to $\boldsymbol{s}_{(\cdot)}$ evaluated in the k^*-th iteration step. The Hessian matrix occurs in

the linearisation of Eq. (11) as well. It contains all second derivatives of $f_{(\cdot)}$, which can be computed (numerically efficient) as analytical expressions analogue to the first derivatives. Morevover, the particular inverse Hessian matrix $\mathbf{H}_{f_{(\cdot)},\boldsymbol{s}_{(\cdot)},k}{}^{-1}$ occurs. Therefore it is necessary, however by no means trivial, to ensure a regular Hessian matrix $\mathbf{H}_{f_{(\cdot)},\boldsymbol{s}_{(\cdot)},k}$ during the entire iteration process. Amongst few strategies, a Levenberg-Marquardt algorithm is applied for parameter identification of the microstructural model. There is a close relation between the choice of design space (model parameters) and the regularity of the Hessian matrix.

For the parameter identification of the hyperelastic model, a Sequential Quadratic Programming algorithm with an Active-Set strategy (e.g. [15, Ch. 18]) is applied, in order to handle constraints in Eq. (5). Initial values are obtained by performing coarse genetic algorithm computations with slightly constrained design spaces.

6.3 Results of parameter identification processes

The design vector for the microstructural model is defined as

$$\boldsymbol{s}_{\mathrm{mic}} = \begin{bmatrix} L_2 & H_1 & H_2 & k_{y,1} & k_{y,2} & c_{N,12} & c_{N,21} & c_{A,1} & c_{A,2} & k_c \end{bmatrix}^T .$$

The reference quantity L_1 is set as $L_1 \coloneqq 1$ in order to perform a numerical computation. As argued on p. 6, there is no need to specify a certain physical unit. The design vector for the hyperelastic model is defined as

$$\boldsymbol{s}_{\mathrm{hyp}} = \begin{bmatrix} c_1 & \varepsilon_1 & \varepsilon_2 & \alpha_1^{(1)} & \alpha_2^{(1)} & \alpha_1^{(2)} & \alpha_2^{(2)} \end{bmatrix}^T .$$

The two analogous optimisation problems (Eq. (10)) are solved as described before. The identified model parameters are (rounded to five digits):

$$\boldsymbol{M}_{\mathrm{mic}}{}^* \coloneqq \begin{bmatrix} \boldsymbol{s}_{\mathrm{mic}}{}^* \\ L_1 \end{bmatrix} = \begin{bmatrix} L_2{}^* \\ H_1{}^* \\ H_2{}^* \\ k_{y,1}{}^* \\ k_{y,2}{}^* \\ c_{N,12}{}^* \\ c_{N,21}{}^* \\ c_{A,1}{}^* \\ c_{A,2}{}^* \\ k_c{}^* \\ L_1 \end{bmatrix} = \begin{bmatrix} 0.78431\ [L_1] \\ 0.10891\ [L_1] \\ 0.073070\ [L_1] \\ 2292.5\ \mathrm{kN} \\ 2132.3\ \mathrm{kN} \\ 18.259\ \mathrm{kN}/[L_1] \\ 16.680\ \mathrm{kN}/[L_1] \\ -115.72\ \mathrm{kN}/[L_1] \\ -90.025\ \mathrm{kN}/[L_1] \\ 162.43\ \mathrm{kN} \\ 1.0 \end{bmatrix}, \quad \boldsymbol{M}_{\mathrm{hyp}}{}^* \coloneqq \begin{bmatrix} c_1{}^* \\ \varepsilon_1{}^* \\ \varepsilon_2{}^* \\ \alpha_1^{(1)*} \\ \alpha_2^{(1)*} \\ \alpha_1^{(2)*} \\ \alpha_2^{(2)*} \end{bmatrix} = \begin{bmatrix} 100.84\ \mathrm{kN/m^2} \\ 473.27\ \mathrm{kN/m^2} \\ 9.6713\ [\text{-}] \\ 326.15\ \mathrm{kN/m^2} \\ 3.2936\ [\text{-}] \\ 294.94\ \mathrm{kN/m^2} \\ 3.3357\ [\text{-}] \end{bmatrix} .$$

The microstructural model with $\boldsymbol{M}_{\mathrm{mic}}{}^*$ is denoted by MATmic, the hyperelastic model with $\boldsymbol{M}_{\mathrm{hyp}}{}^*$ is denoted by MAThyp. Figure 5 shows the load- and stetch curves of the measured data in comparison with the computed results by using material models MATmic resp. MAThyp.

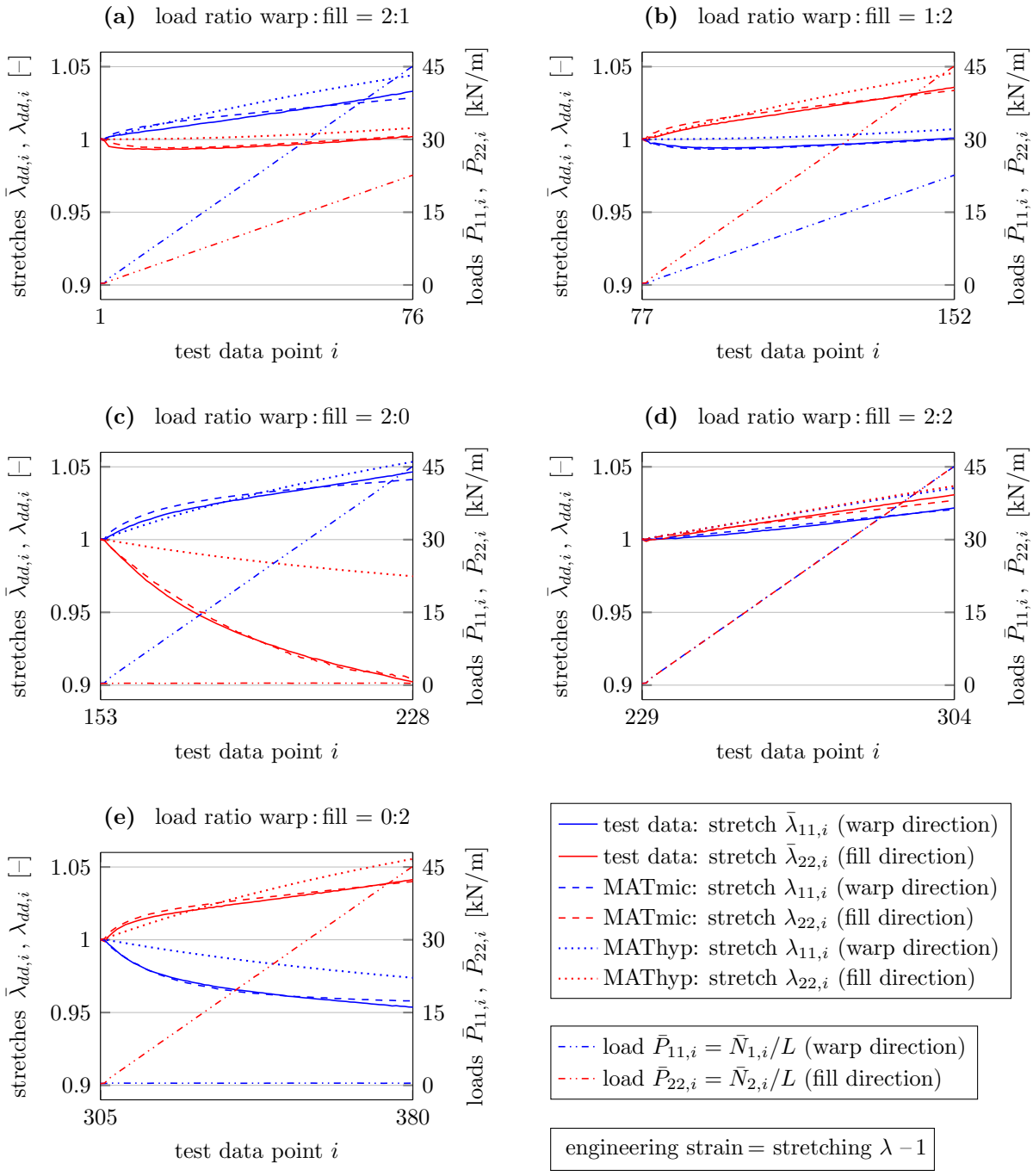

Figure 5: Load- and stretch curves – comparison between measured data from the biaxial tension test and computed results by using material models MATmic resp. MAThyp

7 DISCUSSION

Regarding $\boldsymbol{M}_{\mathrm{mic}}{}^{*}$ the dimensions ${L_2}^{*}$, ${H_1}^{*}$ and ${H_2}^{*}$ show reasonable ratios in comparison to typical dimension ratios of woven fabrics. For example, the height of the microstructural modell ${H_1}^{*} + {H_2}^{*}$ is about a fifth of the dimension L_1. However, a direct physical interpretation of the spring stiffnesses ${c_{A,1}}^{*}$ and ${c_{A,2}}^{*}$ in $\boldsymbol{M}_{\mathrm{mic}}{}^{*}$ (Eq. (12)) is not given (negative values). As long as the input forces F_d are positive (tension forces) the potential of the microstructural model remains strictly convex in u_1, u_2, u_3, u_4 and therefore has one unique minimum (stable equilibrium state). In order to ensure physically interpretable parameter values, one may consider constraining the design space (constrained optimisation). By means of successively leaving out one load ratio in the parameter identification, the microstructural model reveals a satisfying robustness.

Concerning $\boldsymbol{M}_{\mathrm{hyp}}{}^{*}$ the exponents of the anisotropic parts of energy function Eq. (5) ${\alpha_2^{(1)}}^{*}$and ${\alpha_2^{(2)}}^{*}$as well as ${c_1}^{*}$ and ${\varepsilon_2}^{*}$ show values, which fit well in terms of range compared to parameters given in the literature [16, 3].

Considering Figure 5, the measured and computed stretchings with MATmic match well over all considered load ratios. This is confirmed by a coefficient of determination of $R^2 = 0.996$. Hence, the measured data may almost completely be represented by the microstructural model. Comparing the measured and computed stretchings with MAThyp, the representation is widely satisfactory for load ratios 2:0, 2:2 and 0:2, though it is not for load ratios 2:1 and 1:2. This is reflected by a coefficient of determination of R^2=0.604.

The deviations between MAThyp and MATmic are significant. Compared to the chosen hyperelastic model the microstructural model presents a more accurate description of the elastic deformation behaviour. Considering the reasonable effort for the parameter identification the presented microstructural model is a profound and practicable modelling approach.

Part II: An extended numerical approach for form finding and cutting patterning of membranes

1 INTRODUCTION

The common approach of engineering practice is to determine the cutting patterning geometry as a postprocessing step of form finding using a sequence of independent geometrical and mechanical computation steps. Therefore, an incomplete mechanical description between the unstressed cutting patterning and stressed equilibrium geometry exists. Since the equilibrium geometry of the prestressed membrane depends directly on the unstressed cutting patterning geometry, a closed mechanical approach is in demand. Such an approach is developed in the present contribution. In contrast to the approach of Dieringer [8] the presented approach solves the form finding and cutting patterning

problem simultaneously. To this end, two topologically identical meshes are defined. One mesh represents the cutting patterning and the other one the equilibrium geometry. The mechanical behaviour is described by a Total Lagrangian finite element formulation. For the strain-stress relationship the microstructural model derived in Part I is used. The desired stress distribution does not lead to unique geometries of cutting patterning and equilibrium geometry. Defining a least-squares problem of stresses and shear strains as a weighted sum, an optimisation formulation leads to a unique solution. To keep the algorithm numerically stable, the terms that contain the shear strains have to be considerably large. Analogously to the starting point of Update Reference Strategy [4], the presented approach is from a mathematical point of view singular in the tangential plane. Internal nodes of two associated meshes can move without changing any mechanical quantities. Several strategies can be developed to overcome this issue. A robust strategy is to describe the movement of internal nodes of the cutting patterning mesh by means of movement of edge nodes of the same segment. Advantages of this approach are: Firstly, it accounts for the shear deformation of the woven fabric, which occurs during transformation of the plane cutting geometry to the doubly curved surface. Secondly, the ending of membrane fibres at inclined oriented cutting edges is considered. Moreover, it regards material nonlinearities by applying the microstructural model derived in Part I (see Part I, Chapter 4). On the other hand the definition of the seam layout at the beginning of form finding is disadvantageous.

2 OPTIMISATION APPROACH FOR FORM FINDING AND CUTTING PATTERNING OF MEMBRANES

The basic idea of the approach is to formulate an optimisation problem in which both the geometries of the equilibrium and cutting patterning configuration are initially unknown. The two configurations are considered as current resp. reference configuration. The design objectives are minimum deviations from prescribed stresses in warp and fill direction along with minimum shear deformation. The equilibrium equations are introduced into the optimisation problem as equality constraints. Additional design criteria can be formulated (e.g. geometry of seam lines, stress states etc.).

Equilibrium equations are used in Total Lagrange finite element formulation with 4-node membrane elements (see Figure 6). Green Lagrange strains are computed from the deformation gradient in each Gauss point. From this, the stretches of the microstructural model are calculated and a structural analysis is performed. The forces as well as the derivatives of forces of the microstructural model w.r.t. the displacements yield the constitutive equations of the material.

The optimisation problem is

$$\min_{\boldsymbol{s}} f \qquad \text{s. t.} \qquad \boldsymbol{h}(\boldsymbol{s}) = \left[\begin{array}{ccccc} \boldsymbol{R}_{\mathrm{CC}} & \boldsymbol{R}_{\mathrm{RC}} & \boldsymbol{G}_{\mathrm{CC}} & \boldsymbol{G}_{\mathrm{RC}} & \boldsymbol{F}_{\mathrm{CC}} \end{array} \right]^T \stackrel{!}{=} \boldsymbol{0}\,.$$

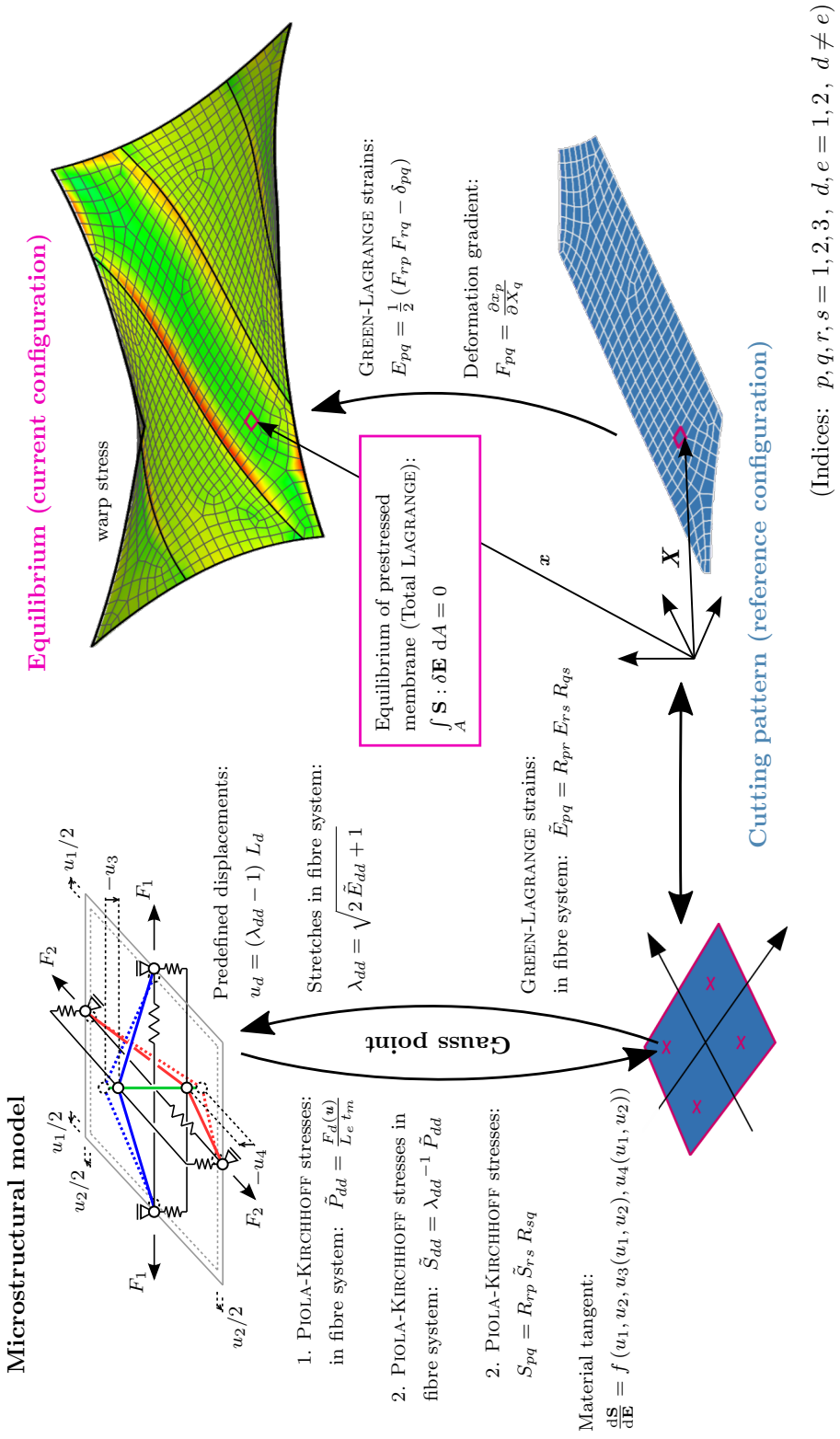

Figure 6: Embedment in finite element approach

The design vector $\boldsymbol{s}$ contains the nodal coordinates of all free nodes in the current configuration as well as those coordinates in the reference configuration that are in the cutting plane. Hence, the dimension of the design space is $\dim \boldsymbol{s} = 3 \cdot n_{n,\mathrm{CC}} + 2 \cdot n_{n,\mathrm{RC}}$.

The objective function of the optimisation problem is:

$$f = f(\boldsymbol{s}) = \sum_{m=1}^{n_\mathrm{G}} \left[w_{11} \left(\tilde{S}_{11,m} - \bar{S}_{11,m} \right)^2 + w_{22} \left(\tilde{S}_{22,m} - \bar{S}_{22,m} \right)^2 + w_{12} \left(\tilde{\phi}_{12,m} - \bar{\phi}_{12,m} \right)^2 \right]$$

$w_{11}, w_{22}, w_{12} \in \mathbb{R}^+$: Weighting factors
$n_{n,\mathrm{RC}}, n_{n,\mathrm{CC}}$: Number of free nodes in the reference resp. current configuration
$\tilde{S}_{11,m}, \tilde{S}_{22,m}$: Computed second Piola-Kirchhoff stresses at Gauss point $m = 1, \ldots, n_\mathrm{G}$
$\bar{S}_{11,m}, \bar{S}_{22,m}$: Prescribed second Piola-Kirchhoff stresses at Gauss point $m = 1, \ldots, n_\mathrm{G}$
$\tilde{\phi}_{12,m}$: Computed shear angle at Gauss point $m = 1, \ldots, n_\mathrm{G}$
$\bar{\phi}_{12,m}$: Prescribed shear angle at Gauss point $m = 1, \ldots, n_\mathrm{G}$

In order to obtain an optimisation problem whose approximation remains regular during computation, further constraints are required along with the equilibrium equations. Amongst others, the following equality constraints $\boldsymbol{h}(\boldsymbol{s})$ are reasonable:

- The Dirichlet boundary conditions in the current configuration;
- the fixation of the reference configuration in plane;
- the geometric position and the equilibrium of the nodes at the inner edges (seam lines) in the current or reference configuration;
- the subdivision of inner as well as free edges.

Avoiding singularities in the tangential plane is explained in the next Section in more detail.

As mentioned, the equilibrium equations are handled as equality constraints. This avoids numerically expensive implicit derivatives. Therefore, it is reasonable to plug first derivatives as well as second derivatives into the optimisation algorithm. Thus, quadratic convergence is achieved under appliance of the algorithm IPOPT [19].

Strategies for stabilisation of cutting configuration

In order to avoid singularities in the tangential plane, several strategies can be used: Firstly, the stabilisation is possible by means of geometrical constraints that demand for elements with (nearly) quadratic shape. This approach gives rise to a multicriteria optimisation. Defining suitable weighting factors is a challenging task. Secondly, movement of inner nodes in the cutting configuration are coupled to movements of edge nodes by using shape basis vectors. This is a common technique to preserve suitable meshes in form

optimisation problems. Thirdly, the movements of the inner nodes can be controlled by formulating an additional mechanical problem. This technique is known as deformation-based shape basis vectors approach in form optimisation and leads to additional equality constraints.

Due to its robustness, the third strategy is used.

3 EXAMPLE

Figure 7 below shows an exemplary conic membrane structure. Due to their curvature, such membranes are characterised by relatively high stresses in warp direction. For the sake of simplicity, the problem is reduced to a quarter model and symmetric boundary conditions are considered.

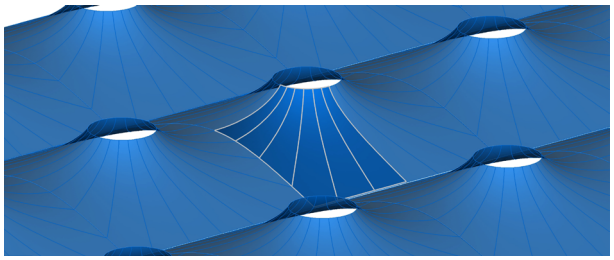

Figure 7: Geometry model of a conic membrane (detail)

Based on the common approach described before, the warp direction is assumed to be radial and the shear deformation is not considered. Though, the necessity of shear deformation in order to obtain a doubly curved surface from plane cutting segments is obvious. Results by using the common approach are compared to results that are obtained applying the approach presented in this contribution. Figure 8a shows the distribution of warp stress while prescribing $\bar{S}_{11,m} = \bar{S}_{22,m} = 4.0$ kN/m^2 in comparison. The results confirm that a homogeneously distributed stress state is not possible when considering the occurence of shear deformation.

As additional load, a uniformly distributed snow load of 0.85 kN/m^2 is imposed. Figure 8b shows the warp stresses in comparison, which reveal major deviations. In the presented approach ending of membrane fibres at the cutting edges are considered, which leads to stress concentrations nearby the cutting edges in the upper zones. In the valley zones of the cutting edges warp yarns withdraw load-carrying and therefore stresses are relatively low. This is caused by the lack of shear stiffness and a slightly destabilising effect due to fill stress.

CONCLUSION

Part I Woven fabric membranes are characterised by a pronounced materially and geometrically nonlinear behaviour. Part I of this contribution focuses on two different material modelling approaches. Firstly, an established microstructural model is presented

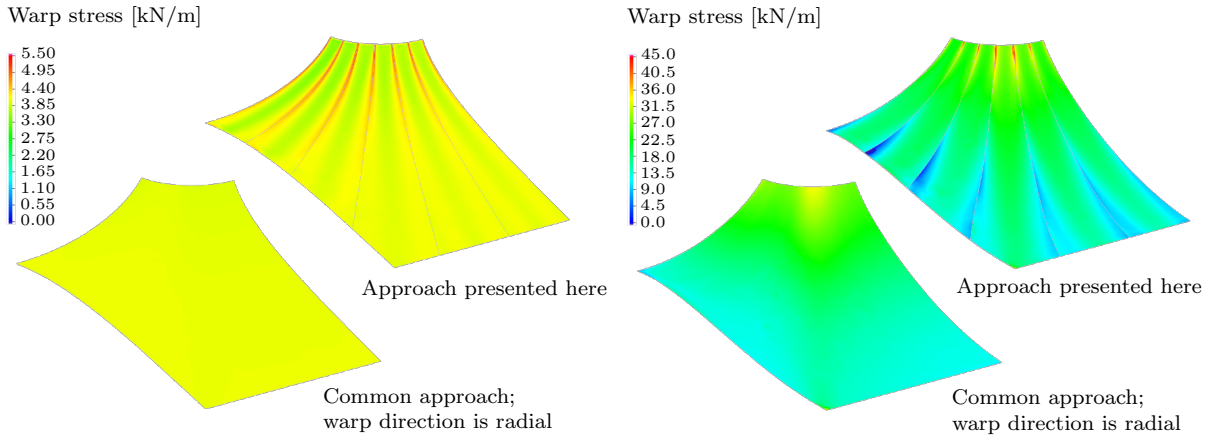

(a) Prescribed stresses $\bar{S}_{11,m} = \bar{S}_{22,m} = 4.0$ kN/m^2 (b) Prescribed stresses and snow load 0.85 kN/m^2

Figure 8: Warp stress [kN/m] – comparison of common approach to approach presented here

and enhanced by introducing transverse spring elements, considering the coating stiffness. Secondly, an established anisotropic hyperelastic model is given. The model parameters of both models are gained by inverse computations w.r.t. to measured data from a biaxial tension test using optimisation. Comparing the results of the microstructural model and the chosen anisotropic hyperelastic material model, the microstructural model is assessed as more suitable. Using a different energy function for the hyperelastic model could probably improve results of this approach. Moreover, using a larger test data set would be an interesting task in order to ensure robustness.

Part II In order to consider effects arising from nonlinear material behaviour, from shear deformation of the woven fabric during transformation in a doubly curved surface as well as from ending of material fibres at the cutting edges, form finding and cutting patterning has to be treated in a coupled computation. The present contribution presents an approach for consideration of the coupled problem as an optimisation problem, in which both the reference as well as the current configuration are initially unknown. In order to avoid singularity in the tangential plane of the surface, a shape basis vector technique is applied.

Based on an exemplary conic membrane structure, major deviations of the common approach in comparison to the presented approach are revealed.

ACKNOWLEDGEMENT

The work has been partially funded by German Research Foundation (DFG) as a part of the Collaborative Research Centre (SFB) 1244 "Adaptive Envelopes and Structures for the Built Environment of the Future"/project A04 under grant number SFB 1244/1 2017. Moreover, thanks to Dipl.-Ing. Katja Bernert from Low and Bonar GmbH (former Mehler Texnologies GmbH, Fulda/Germany) for providing the test data from the biaxial tension test.

REFERENCES

[1] Ballhause, D.: *Diskrete Modellierung des Verformungs- und Versagensverhaltens von Gewebemembranen.* Dissertation, Universität Stuttgart, 2007.

[2] Balzani, D.; Neff, P.; Schröder, J.; Holzapfel, G. A.: *A polyconvex framework for soft biological tissues. Adjustment to experimental data.* International Journal of Solids and Structures 43(2006), pp. 6052-6070.

[3] Balzani, D.; Gruttmann, F.; Schröder, J.: *Analysis of thin shells using anisotropic polyconvex energy densities.* Computer Methods in Applied Mechanics and Engineering 197(2008), pp. 1015-1032.

[4] Bletzinger, K.-U.; Ramm, E.: *A general finite element approach to the form finding of tensile structures by the updated reference strategy.* International Journal of Space Structures 14, 2(1999), pp. 131–145.

[5] Blum, R.; Bidmon, W.: *Spannungs-Dehnungs-Verhalten von Bautextilien: Theorie und Experiment.* SFB 64, Mitteilungen 74/1987, Universität Stuttgart, 1987.

[6] Bögner, H.: *Vorgespannte Konstruktionen aus beschichteten Geweben und die Rolle des Schubverhaltens bei der Bildung von zweifach gekrümmten Flächen aus ebenen Streifen.* Dissertation, Institut für Werkstoffe im Bauwesen der Universität Stuttgart, 2004

[7] Bridgens, B.; Gosling, P. D.: *Interpretation of results from the MSAJ 'Testing Method for Elastic Constants of Membrane Materials'.* In: Oñate, E.; Kröplin, B. (Eds.): *Proc. of et Symposium.* Sofia, 2010, pp. 49–57.

[8] Dieringer, F. H.: *Numerical Methods for the Design and Analysis of Tensile Structures.* Dissertation, Lehrstuhl für Statik, Technische Universität München, 2014

[9] Feyel, F.: *A multilevel finite element method (FE^2) to describe the response of highly non-linear structures using generalized continua.* Computer Methods in Applied Mechanics and Engineering 192, 28–30(2003), pp. 3233–3244.

[10] Holzapfel, G. A.: *Nonlinear Solid Mechanics. A Continuum Approach for Engineering.* John Wiley & Sons Ltd, Chichester, England, 2000.

[11] Kaiser, B.; Haug, E.; Pyttel, T.; Duddeck, F.: *A generalized coupled multi-scale approach for the simulation of textile membranes.* In: Oñate, E.; Bletzinger, K.-U.; Kröplin, B. H. (Hrsg.): *VII International Conference on Textile Composites and Inflatable Structures.* Barcelona/Spain, 2015, pp. 433–444

[12] Kawabata, S.; Niwa, M.; Kawai, H.: *The finite-deformation theory of plain-weave fabrics Part I: The biaxial-deformation theory.* The Journal of the Textile Institute 64, 1(1973), pp. 21–46.

[13] Meffert, B.: *Mechanische Eigenschaften PVC-beschichteter Polyestergewebe.* Dissertation, Fakultät für Maschinenwesen der Rheinisch-Westfälischen Technischen Hochschule Aachen, 1978

[14] Membrane Structures Association of Japan: *MSAJ/M-02-1995: Testing Method for Elastic Constants of Membrane Materials.* 1995.

[15] Nocedal, J.; Wright, S. J.: *Numerical Optimization.* Springer, New York, NY, USA, 2nd edition, 2006.

[16] Schröder, J.; Balzani, D.; Stranghöner, N.; Uhlemann, J.; Gruttmann, F.; Saxe, K.: *Membranstrukturen mit nicht-linearem anisotropem Materialverhalten - Aspekte der Materialprüfung und der numerischen Simulation.* Der Bauingenieur 86, 9(2011), pp. 381–389

[17] Schröder, J.; Balzani, D.; Niesters, C.: *Modellierung dünner Schalen mit hyperelastischem Materialverhalten.* Essener Membranbau Symposium 2014, Essen, 2014.

[18] Uhlemann, J.; Stranghöner, N.: *Einfluss fiktiver elastischer Konstanten von textilen Gewebemembranen in der Tragwerksanalyse von Membranstrukturen.* Stahlbau 82, 9(2013), pp. 643–651.

[19] Wächter, A.; Biegler, L. T.: *On the Implementation of a Primal-Dual Interior Point Filter Line Search Algorithm for Large-Scale Nonlinear Programming.* Mathematical Programming 106, 1(2006), pp. 25–57.